Cancer Research

Grapefruit-Derived Nanovectors Use an Activated Leukocyte Trafficking Pathway to Deliver Therapeutic Agents to Inflammatory Tumor Sites

Qilong Wang[1,2], Yi Ren[3], Jingyao Mu[2], Nejat K. Egilmez[2], Xiaoyin Zhuang[4], Zhongbin Deng[4], Lifeng Zhang[4], Jun Yan[4], Donald Miller[4], and Huang-Ge Zhang[1,2]

Abstract

Inflammation is a hallmark of cancer. Activated immune cells are intrinsically capable of homing to inflammatory sites. Using three inflammatory-driven disease mouse models, we show that grapefruit-derived nanovectors (GNV) coated with inflammatory-related receptor enriched membranes of activated leukocytes (IGNVs) are enhanced for homing to inflammatory tumor tissues. Blocking LFA-1 or CXCR1 and CXCR2 on the IGNVs significantly inhibits IGNV homing to the inflammatory tissue. The therapeutic potential of IGNVs was further demonstrated by enhancing the chemotherapeutic effect as shown by inhibition of tumor growth in two tumor models and inhibiting the inflammatory effects of dextran sulfate sodium-induced mouse colitis. The fact that IGNVs are capable of homing to inflammatory tissue and that chemokines are overexpressed in diseased human tissue provides the rationale for using IGNVs to more directly deliver therapeutic agents to inflammatory tumor sites and the rationale for the use of IGNVs as treatment for certain cancers in personalized medicine. *Cancer Res; 75(12); 2520–9. ©2015 AACR.*

Introduction

Inflammation is a hallmark of most diseases, including cancer, autoimmune disease, and infectious disease. The development of target-specific delivery systems to inflammatory sites is needed urgently. The attraction of leukocytes, including T cells, to sites of inflammation and infection is an essential component of the host response to disease, including autoimmune and chronic inflammatory diseases as well as infectious disease and cancer. Recruitment of circulating T cells to sites of pathogen entry or inflammation involves at least two separate migration processes, termed extravasation and chemotaxis. Adhesion to the luminal side of blood vessels, trans-endothelial migration, and subsequent chemotaxis of leucocytes are highly complex processes (1, 2). Chemokines and their receptors play a coordinating role in both the homeostatic circulation of T cells, as well as their movement to sites of inflammation or injury (1–4). Once T cells are within inflammatory tissue, their response can be affected by the many inflammatory chemokines that are overexpressed and have broad target cell selectivity (5–9). The fact that there is a redundancy within the chemokine network with respect to ligand–receptor binding and that an array of chemokines is overexpressed by a variety of cells in inflammatory tissues makes the use of chemokines a potential component for the development of therapeutic targeting.

For a therapeutic agent to exert its desired effect, it needs to (1) reach the desired site and (2) be in physical contact with its target. The development of target-specific delivery systems has not yet been broadly successful. Despite many potential advantages for using nanoparticles (10) and liposomes, hurdles to their use include cytotoxicity, induction of chronic inflammation, host immune responses, difficulties of large scale production at affordable prices, and potential biohazards to the environment (11, 12). Unlike the situation with artificially synthesized nanoparticles, naturally released nano-sized exosomes derived from many different types of mammalian cells play an important role in intercellular communication. Nano-sized exosomes released from mammalian cells have been utilized for encapsulating drugs Stat3 inhibitor JSI-124 (12.5 pmol) and curcumin (1.5 nmol; ref. 13) and siRNA (14) to treat diseases in mouse disease models without side effects. Although this approach is promising, production of large quantities of mammalian cell nanoparticles and evaluation of their potential biohazards have been challenging. We have identified recently exosome-like nanoparticles from the tissue of edible plants, including grapefruit, grapes, and tomatoes, and produced them in large quantities (15–17). As with mammalian exosomes, we have demonstrated that exosome-like nanoparticles from grapes naturally encapsulate small RNAs, proteins, and lipids. Using both *in vitro* cell culture models as well as mouse models, we have shown that grapefruit -derived nanovectors (GNV) are highly efficient for delivering a variety of therapeutic agents, including drugs, DNA expression vectors, siRNA, and antibody (18). In this study, we set out to determine whether the binding of inflammatory cell-derived membranes on grapefruit GNVs would be an efficient strategy to take

[1]Louisville Veterans Administration Medical Center, Louisville, Kentucky. [2]James Brown Cancer Center, Department of Microbiology and Immunology, University of Louisville, Louisville, Kentucky. [3]Department of Breast and Thyroid Surgery, Huai'an First People's Hospital, Huai'an, Jiangsu, China. [4]James Brown Cancer Center, Department of Medicine, University of Louisville, Louisville, Kentucky.

Note: Supplementary data for this article are available at Cancer Research Online (http://cancerres.aacrjournals.org/).

Corresponding Author: Huang-Ge Zhang, Brown Cancer Center, University of Louisville, CTRB 309, 505 Hancock Street, Louisville, KY 40202. Phone: 502-852-8623; Fax: 502-852-3842; E-mail: H0Zhan17@louisville.edu

doi: 10.1158/0008-5472.CAN-14-3095

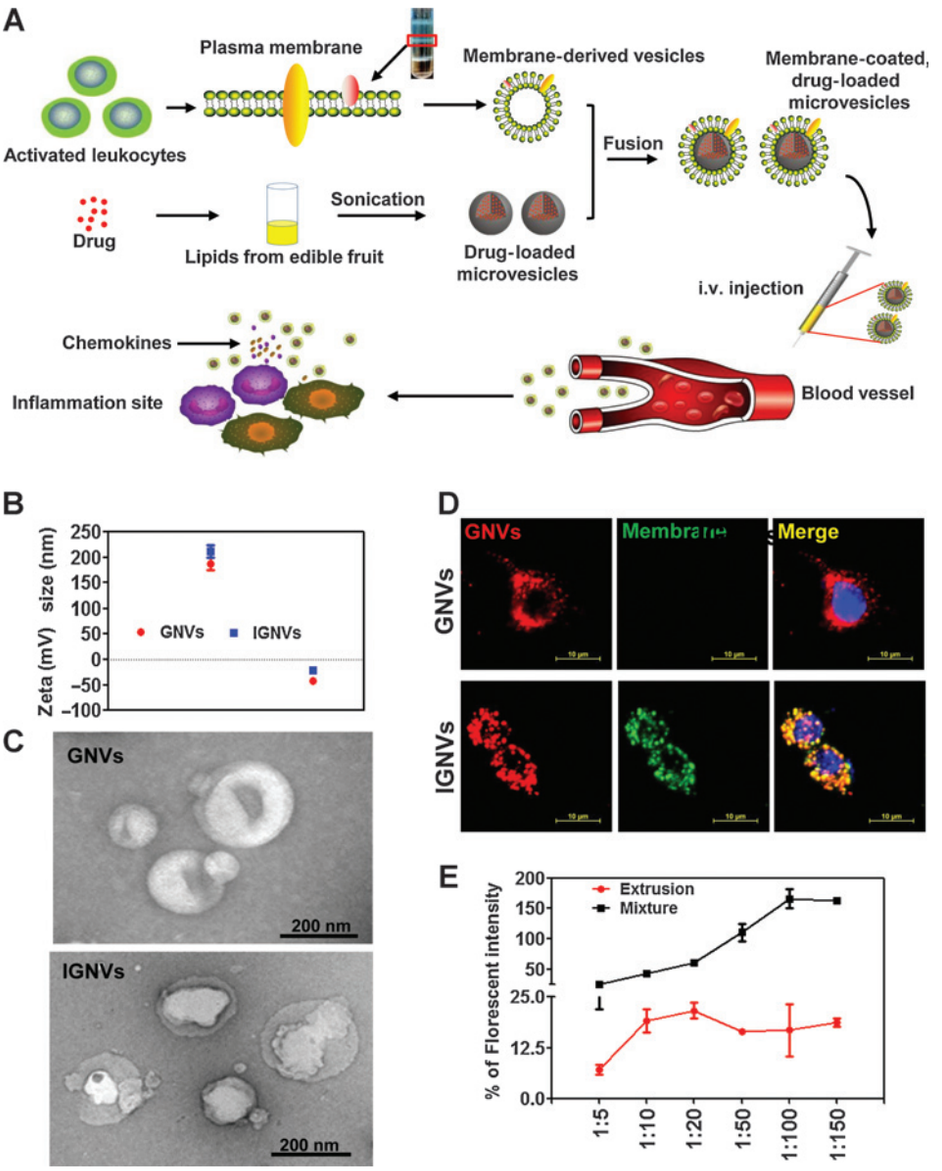

Figure 1.
Characterization of plasma membrane-coated GNVs (IGNVs). A, schematics of the preparation process of the IGNVs and drug loaded-GNV microvesicles for targeted delivery of therapeutic agents to inflammatory sites. B, size distribution and surface Zeta potential of free GNVs (red) and EL4 cells plasma membrane-coated GNVs (IGNVs, blue) were measured using a ZetaSizer. C, free GNVs (top) and IGNVs (bottom) were visualized and imaged by scanning electron microscopy. D, the colocalization of the EL4 cell-derived plasma membranes and GNV cores. For assembling IGNVs, the EL4 cell-derived plasma membranes were labeled with PKH67 green dye and GNV cores were labeled with PKH26 red dye. 4T1 cells were cultured in the presence of GNVs (top) or IGNVs (bottom) for 12 hours. Representative images of cells were then taken using a confocal microscope at a magnification of ×400. E, FRET-based measurements of IGNV formation. DiO-labeled GNVs and DPA-labeled membrane vesicles ($n = 3$) were mixed, and subsequently the mixture was extruded 20 times through a 200-nm polycarbonate porous membrane using an Avanti mini extruder or the mixture without further extrusion was used as a control. The extruded products and the mixed products were then diluted and the intensity of fluorescence was measured. Data (B, C, D, and E) are representative of three independent experiments.

advantage of the unlimited availability of GNVs and to generate personalized delivery vectors that would target inflammatory sites in diseases we are investigating (Fig. 1A). Our hypothetical model (Fig. 1A) has two advanced features that we sought to prove in this study: (i) plasma membrane from activated leukocytes is easily and preferentially bound on the microvesicles made of fruit nanoparticles lipids and (ii) the resultant microvesicles are safe and can be successfully used for targeted delivery of therapeutic agents to inflammatory sites. As proof of concept, we used GNVs as an example since the data from our previous publication (18) suggested that GNVs are nontoxic and are capable of carrying a number of different types of therapeutic agents. Also, because multiple factors are involved in the attraction of leukocytes, including T cells, to sites of inflammation, and chemokines/chemokine receptors play an important role in the last step of activated leukocyte homing to inflammatory sites, the role of IGNVs chemokines/chemokine receptors for targeted delivery was investigated as a proof of concept.

Materials and Methods

Cell culture

The mouse T-lymphoma EL4 cells, mouse 4T1, 4TO7 breast cancer cell lines, mouse NMuMG mammary gland epithelial cells, CT26 colon cancer, and human umbilical vein endothelial cells (HUVEC) were purchased from ATCC. CT26 cells were cultured in RPMI-1640 media; EL4, 4T1, and 4TO7 cells were maintained in DMEM media supplemented with 10% heat-inactivated FBS. HUVECs were cultured in complete endothelial cell growth medium (ECGM; Promocell #C-22010). NMuMG cells were cultured in complete DMEM media supplemented with 10 μg/mL insulin. All cells were maintained in a humidified CO_2 incubator at 37°C.

Plasma membrane isolation and purification

Plasma membranes were isolated and purified using a method as described (10). In brief, mouse lymphoma cell line EL4 cells were cultured with/without phorbol 12-myristate 13-acetate (PMA) stimulation (100 ng/mL) for 12 hours. Cells (2×10^8) were then collected and centrifuged at 500 g for 10 minutes at 4°C. The cell pellets were resuspended in 1 mL of homogenization buffer at a final concentration of 10 mmol/L Tris.HCL, 25 mmol/L D-sucrose, 1 mmol/L $MgCL_2$, 1 mmol/L KCL, 10 μg/mL RNase, 10 μg/mL DNase, and 1× proteinase inhibitor cocktail. The cell suspension was homogenized on ice by 100 passes using a hand-held Dounce homogenizer. The supernatant was collected after centrifugation at 500 g for 10 minutes. For further purification, collected supernatants were subjected to a discontinuous sucrose density gradient centrifugation at 28,000 g for 45 minutes at 4°C on a 30%, 40%, and 55% sucrose in a 0.9% saline solution. For plasma membrane isolation from leukocytes of mice or human peripheral blood, anticoagulant-treated peripheral blood was collected and centrifuged at 3000 g for 10 minutes at 4°C. Leukocytes were collected and the red blood cells were lysed by incubation with ACK lysis buffer (NH_4CL 8.024 g/L, $KHCO_3$ 1g/L, EDTA-2Na 3.722 mg/L) for 5 minutes at 22°C. The procedure for lysis of red blood cells was repeated once. The leukocytes were then cultured in RPMI-1640 with lipopolysaccharide (LPS; 100 ng/mL) for 12 hours before the plasma membranes from leukocytes of mice or human with/without LPS stimulation were isolated and purified using a discontinuous sucrose density gradient centrifugation method as described above.

Preparation of plasma membrane-derived vesicles

The plasma membranes purified from EL4 cells and mice or human peripheral blood leucocytes were sonicated in a glass vial with 200 μL ddH_2O for 10 minutes using a FS30D bath sonicator (Fisher Scientific). The resulting vesicles were subsequently extruded through 100 nm polycarbonate porous membranes using an Avanti mini extruder (Avanti Polar Lipids).

Preparation of plasma membrane-coated GNVs

Grapefruit lipid-derived nanoparticles (GNV) were prepared according to the protocol as described in our previous publication (17). To prepare the plasma membrane-coated GNVs, 400 nmol of GNVs were mixed with plasma membrane-derived vesicles (from $\sim 5 \times 10^5$ cells) and extruded 20 times through a 200-nm polycarbonate porous membrane using an Avanti mini extruder. Henceforth, the GNVs coated with EL4-derived or mouse or human leukocyte-derived plasma membranes are referred to as pseudo-inflammatory GNVs (IGNVs). Details of other methods used in this study are described in the Supplementary Experimental Procedures.

Statistical analysis

One-way ANOVA followed by Turkey *post hoc* tests was used to determine the differences occurred between groups, and *t* test was used to determine the difference between two groups (*, $P < 0.05$; **, $P < 0.01$; and ***, $P < 0.001$).

Results

Characterization of GNVs coated with inflammatory chemokine receptor enriched membrane fraction of activated T cells (IGNVs)

IGNVs were generated by binding membranes derived from the PMA-activated EL4 T-cell line to GNVs. Morphology (Supplementary Fig. S1A) and quantity of chemokine receptors (Supplementary Fig. S1B) of EL4 T cells stimulated with/without PMA were analyzed. Vesicles from the purified middle band of a sucrose gradient (Supplementary Fig. S2A) were prepared by extrusion and subsequently bound with GNVs. The Zeta potential and size distribution of IGNVs were then analyzed (Fig. 1B). Transmission electron microscopy imaging (Fig. 1C) indicated that IGNVs had a similar morphology of GNVs. IGNVs were internalized by CT26 colon cancer cells in a similar manner as GNVs (Fig. 1D), and colocalized with EL4 membrane (Fig. 1D, last column). Simple mixing of GNVs with EL4 cell-derived membrane vesicles did not result in colocalization in transfected 4T1 cells (Supplementary Fig. S2B). Fluorescence resonance energy transfer (FRET) analysis further confirmed that more than 83 ± 2.2% of the GNVs were coated with plasma membrane from activated EL4 T cells (IGNVs; Fig. 1E). After preparation and through 5 days at 22°C (Supplementary Fig. S2C) or 25 hours at 37°C (Supplementary Fig. S2D), the IGNVs were stable without significant changes in size or charge.

IGNVs home to inflammatory sites

Next, to determine whether IGNVs would leave the peripheral circulation and home to inflammatory tissues, three inflammatory mouse models were tested. We first sought to determine whether IGNVs transmigrated through a HUVEC monolayer at a higher efficiency than GNVs by using an *in vitro* Transwell assay. The data demonstrated that much higher numbers of IGNVs-transfected HUVECs ($DAPI^+PKH26^+$; data not shown) migrated to the bottom of the Transwell (right) than did GNVs (left) over a 48-hour period (Fig. 2A). Addition of chemokines (CXCL1/2/9/10, CCL2/5) in the bottom of the Transwell further enhanced the efficiency of IGNV transmigration (Fig. 2A; right, 4th column; **, $P < 0.01$). Enhanced homing of IGNVs to inflammatory sites when compared with GNVs was further confirmed in different inflammatory models, two acute inflammation models [a LPS-induced skin inflammation (Fig. 2B) and dextran sulfate sodium (DSS)-induced colitis model (Fig. 2C; **, $P < 0.01$)] and two chronic inflammation cancer models [the CT26 colon cancer (Fig. 2D; ***, $P < 0.001$] and 4T1 breast cancer models (Fig. 2E; ***, $P < 0.001$).

CXCR2 and LFA-1 play a key role in IGNV homing

Leukocyte recruitment into inflamed tissue follows a well-defined cascade of events, beginning with capturing of free flowing leukocytes to the vessel wall, followed by rolling, adhesion to endothelial cells, post-adhesion strengthening, crawling, and finally transmigration through endothelial junctions into sites of inflammation. During these steps, chemokines/chemokine receptors play a key role in the last step, transmigration. We therefore analyzed the profiles of chemokines from the extracts of inflammatory tissues and the types of chemokine receptors coated on the IGNVs. Chemokine array data (Fig. 3A) indicated that chemokines identified are in much higher concentrations in the extracts of the inflammation models we tested than the extracts from nontumor mammary gland (Fig. 3A, normal). We also noticed, in general, that stronger chemokine signals were detected in the extracts from 4T1 breast tumor than from the skin of LPS-induced skin inflammation or CT26 colon tumor. FACS analysis data indicated that corresponding receptors of chemokines are detected on the IGNVs (Fig. 3B). To determine which

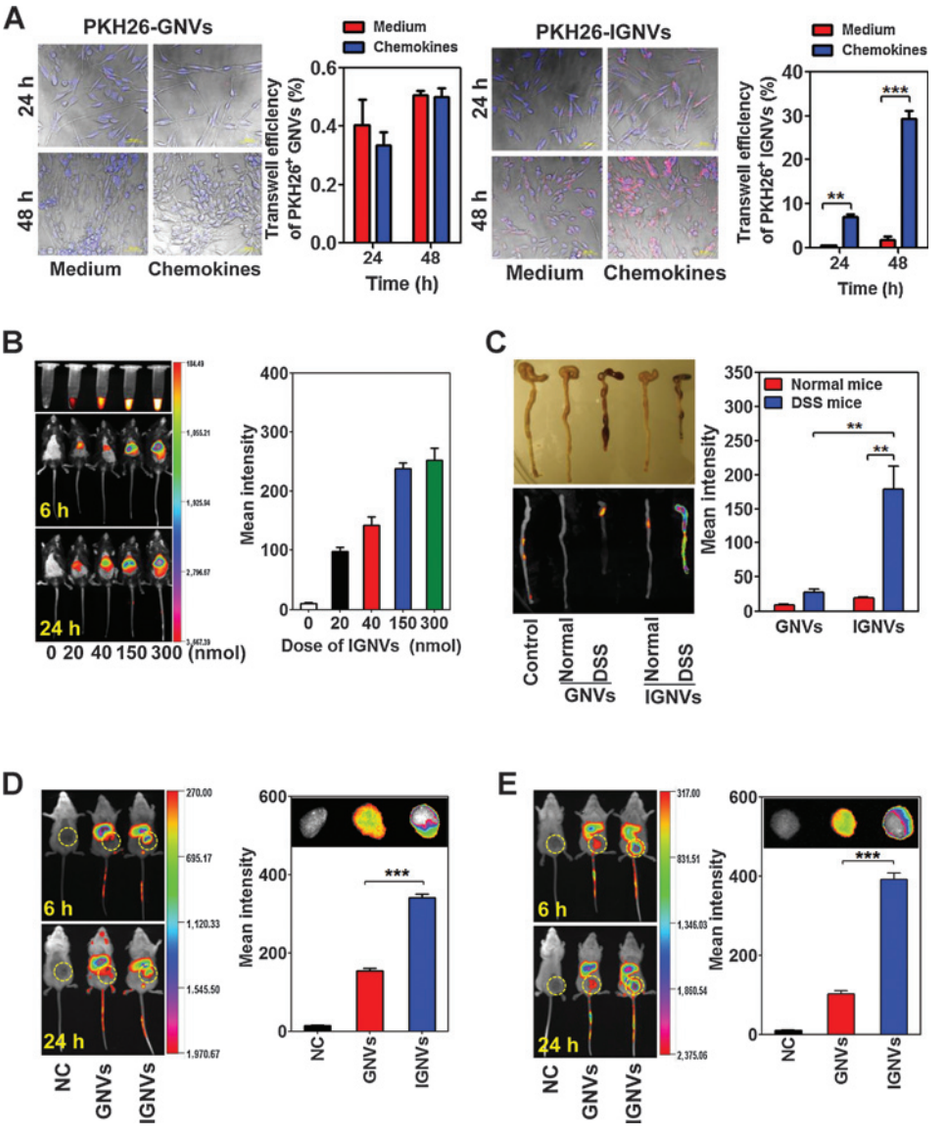

Figure 2.
IGNVs utilize the activated leukocyte membrane-dependent pathways and efficiently target delivery of IGNVs to inflammatory sites. A, Transwell assay for detecting chemotaxis of EL4 cell plasma membrane-coated GNVs. HUVEC cells were cultured in the upper chamber and 4TO7 cells were cultured in the lower chamber of a Transwell plate. Transmigration of the PKH26 (red)-labeled GNVs or IGNVs were imaged after 24 and 48 hours in culture using a confocal microscope. The intensity of the fluorescent signal of media in the lower chamber ($n = 3$) was measured and expressed as the percentage of Transwell efficiency of fluorescent intensity of PKH26-labeled GNVs or IGNVs. Data are representative of three independent experiments. Distribution of DiR dye-labeled IGNVs in: LPS-induced skin acute inflammatory mouse model (B); DSS-induced colitis mice (C); CT26 tumor model (D); and 4T1 tumor model (E). Live-mouse images (left) were collected 6 and 24 hours after i.v. injection of DiR dye-labeled IGNVs. Skin, colon, and tumor tissues were removed 24 hours after the injection and scanned for DiR dye signals. A representative image from each group of mice is shown (left) and followed by graphical figures (right) presented as the mean net intensity (sum Intensity/area, $n = 5$). **, $P < 0.01$ and ***, $P < 0.001$. Data are representative of at least five independent experiments.

chemokine(s) in the inflammatory tissues play a causative role in recruiting IGNVs into the inflammatory tissue, an *in vitro* Transwell assay was conducted. The results indicated that the transmigration of IGNVs was affected in a remarkable way by addition of chemokines into the bottom of the Transwells, whereas, there was no change in GNV migration with the addition of chemokines. Addition of CXCL1 or CXCL2 resulted in more IGNVs detected in the bottom of the well 48 hours post-addition, and the combination of chemokines, CXCL1/2/9/10/CCL2/5 led to the highest efficiency in transmigration of IGNVs (Supplementary Fig. S3). The effects of chemokines on IGNVs transmigration were then confirmed by the results generated from a neutralizing chemokine assay. Although preincubation with recombinant chemokine against each chemokine receptor partially attenuated the migration of IGNVs, neutralizing all six chemokine receptors as listed or preincubation with 4T1 tumor extract led to a maximum reduction of IGNVs transmigration (Fig. 3C; *, $P < 0.05$; **, $P < 0.01$; and ***, $P < 0.001$). This reduction was also confirmed in a LPS-induced skin inflammation model in mice where the mice were i.v. injected with DiR dye-labeled IGNVs that had been preincubated with 4T1 tumor extract (Fig. 3D; **, $P < 0.01$).

The data generated from a 24-hour (time course was determined based on the data from Fig. 3D) *in vivo* imaging analysis further confirmed that although CXCL1, CCL2, and CCL5 have an effect, CXCL2 plays a key role in homing IGNVs into inflammatory sites, including LPS-induced acute inflammation in skin (Fig. 3F; *, $P < 0.05$; **, $P < 0.01$; and ***, $P < 0.001$) and the CT26 colon cancer model (Fig. 3G; *, $P < 0.05$; **, $P < 0.01$; and ***, $P < 0.001$).

Integrins, including LFA-1 and α4β7, have multiple functions in the process of leukocyte recruitment from initially adhering to vessel walls to crawling before the final step, transmigration. FACS data indicated that although no α4β7 was detected, LFA-1 was highly expressed on both PMA-activated EL4 cells (Supplementary Fig. S4A) and present on IGNVs (Supplementary Fig. S4B). Transmigration of IGNVs was dramatically decreased *in vitro* (Fig. 3H; ***, $P < 0.001$) and *in vivo* (Fig. 3I; *, $P < 0.05$) when LFA-1 on IGNVs was neutralized. Because multiple factors, including LFA-1, play a role in the process of leukocytes and

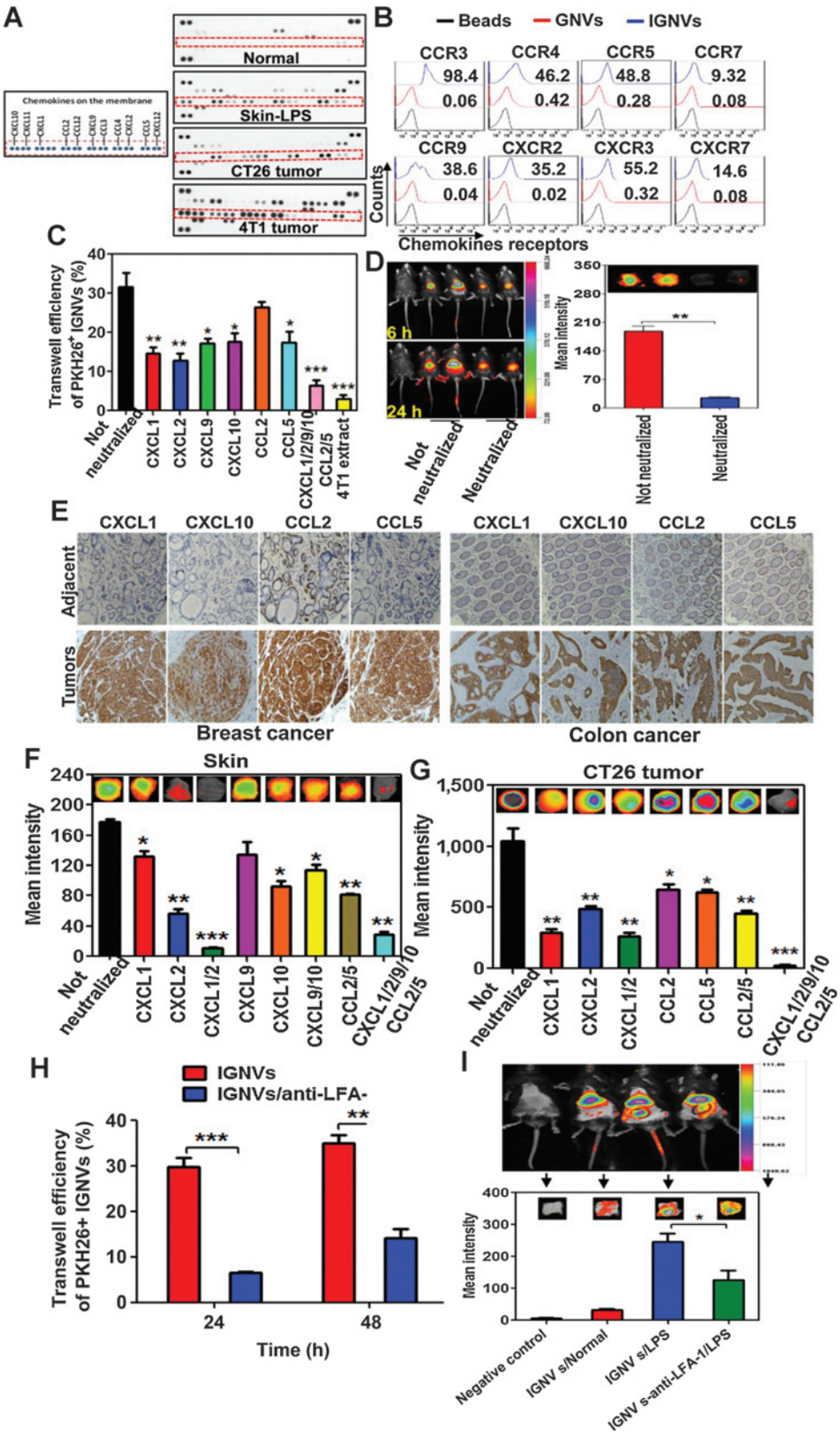

nanoparticles (10) homing to inflammatory sites, and chemokines/chemokine receptors have been known to play important roles in the last step (transmigration) of leukocyte homing to inflammatory tissue in general, for proof of concept in this study, chemokine-related assays were used as a primary determinant of function without further analysis of the role of IGNV LFA-1.

We further determined whether the chemokines of interest were upregulated in human cancer tissues. The results from immunohistological staining of chemokines in human breast cancer (Supplementary Table S1) and colon cancer (Supplementary Table S2) suggest a much higher expression of CXCL1, CXCL10, CCL2, and CCL5 in tumor tissues than in adjacent nontumor tissues (Fig. 3E and Supplementary Tables S3 and S4).

To further demonstrate whether this approach can be applied for treatment of patients in a personalized manner, GNVs coated with the membrane of LPS stimulated leukocytes isolated from the peripheral blood of healthy human subjects (Supplementary Fig. S5A) or of mice (Supplementary Fig. S5B) were purified using a sucrose gradient. The chemokine receptors on the IGNVs were quantitatively analyzed (Fig. 4A and B). We then determined whether IGNVs are capable of homing to human tumor using the human colon SW620 tumor model because the chemokines of interest are overexpressed in human colon cancer, as well as breast tumor tissue, and are also released from SW620 colon cancer cells (Supplementary Fig. S5C; ***, $P < 0.001$). The results from *in vivo* imaging analysis indicate that human SW620 tumor-bearing mice (Fig. 4C; **, $P < 0.01$) or mice locally challenged with LPS (Fig. 4D; *, $P < 0.05$ and ***, $P < 0.001$) attracted more IGNVs than GNVs, and IGNVs coated with purified membranes of LPS-stimulated leukocytes have the highest fluorescent intensity day 5 after i.v. injection. The results from an *in vitro* Transwell assay (Fig. 3C) further stimulated us to further determine whether CXCR2 plays a dominant role in IGNV homing to the inflammatory site. The results generated from *in vivo* imaging analysis indicate that IGNVs coated with the membrane of LPS-stimulated leukocytes isolated from the peripheral blood of CXCR2 knockout mice had significantly attenuated the migration of IGNVs to the inflammatory site (Fig. 4E), suggesting that IGNV CXCR2 plays a key role in IGNV homing.

In vivo therapeutic effects of drugs carried by IGNVs

Because no adverse side-effects had been observed with an i.v. injection of IGNVs (Supplementary Fig. S6), we tested whether IGNVs can be used as a therapeutic drug delivery vehicle. IGNVs are capable of being loaded with different drugs, including chemo drugs, such as doxorubicin, and anti-inflammatory agents like curcumin (Supplementary Fig. S7A). Both doxorubicin and curcumin-loaded IGNVs have a similar Zeta potential and size distribution (Supplementary Fig. S7B and S7C) although the loading capacity (Supplementary Fig. S7D) and releasing of an agent (Supplementary Fig. S7E) are different for different types of agents. Further analysis of the stability of IGNVs indicated that circulating IGNVs were stable and detectable until day 5 (Fig. 5A) after an i.v. injection, which in turn provides a longer time span for IGNVs to home to where inflammation is occurring. In addition, IGNV-DOX was stable without an increase of releasing doxorubicin until they were in a pH 5.5 (Fig. 5B; **, $P < 0.01$). In contrast, a pH as low as 5.0 did not result in the increase of releasing doxorubicin from commercially available doxorubicin-loaded liposomes (Supplementary Fig. S7F), although there were no differences observed in the cell cytotoxicity (Supplementary Fig. S7G), *in vivo* induction of proinflammatory cytokines (Supplementary Fig. S7H), and the release of liver enzymes (Supplementary Fig. S7I) between IGNVs (Supplementary Fig. S6D) and control liposomes. The tissue distribution of doxorubicin encapsulated into IGNVs was determined next. The concentration of doxorubicin was higher in the tumor and lower in the liver of tumor-bearing mice i.v. injected with IGNV-DOX when compared with DOX-NP-treated mice (Fig. 5C; *, $P < 0.05$). This result was further confirmed by the much stronger intensity of doxorubicin signals detected in the CT26 tumor as well as 4T1 breast tumor-bearing mice i.v. injected with IGNV-DOX when compared with mice treated with GNV-DOX or free doxorubicin (Fig. 5D). Injection of GNV-DOX mixed with EL4 cell-derived membrane vesicles had significantly lower levels of doxorubicin detected in the 4T1 tumor than IGNV-DOX (Supplementary Fig. S8A), suggesting that the extrusion of GNVs with the activated leukocyte membranes, which leads to formation of

Figure 3.

Chemokine-mediated pathways play a causative role in efficient targeted delivery of IGNVs to inflammatory sites. A, chemokine expression in normal skin (normal), LPS-induced acute inflammatory skin tissues (Skin-LPS), CT26 (CT26 tumor), and 4T1 (4T1 tumor) were determined using the Proteome Profiler from R&D Systems. Each dot represents a chemokine detected by a capture antibody and printed in duplicate on the membrane. B, expression of chemokine receptors on IGNVs was analyzed by FACS analysis of IGNVs coated on 4-μm diameter aldehyde/sulfate latex beads. A representative image ($n = 5$) from each sample is shown. C, *in vitro* transmigration of IGNVs. HUVEC cells ($n = 3$) were cultured in the fibronectin-coated upper chamber as a transmigration barrier. PKH26-labeled IGNVs (PKH26-IGNVs) were preincubated with recombinant chemokines as listed in Fig. 3C or with the extract from 4T1 tumor. After washing, preincubated PKH26-IGNVs were added to the upper chamber and cultured in the presence of recombinant chemokines (CXCL1/2/9/10 plus CCL2/5) in the lower chamber. After a 24-hour incubation, the intensity of PKH26 fluorescence of media in the lower chamber ($n = 3$) was measured and expressed as the percentage of Transwell efficiency of $PKH26^+$ IGNVs. D, images of IGNVs in LPS-induced acute skin inflammatory mice. DiR dye-labeled IGNVs were preincubated overnight at 4°C with (neutralized) or without (not neutralized) 4T1 extract before an i.v. injection. A representative image at 6 and 24 hours after the injection from each group of mice ($n = 5$) is shown (left) and followed by graphical figures (right) presented as the mean net intensity (sum intensity/area, $n = 5$). Data are representative of at least three independent experiments. E, IHC staining of chemokines (CCL2, CCL5, CXCL9, and CXCL10) expressed in human breast cancer, colon cancer tissues (bottom), and paired adjacent tissues (upper panels). A representative image ($n = 20$ for colon cancer; $n = 21$ for breast cancer) from each sample is shown. DiR dye-labeled IGNVs were preincubated at 4°C overnight with recombinant chemokines as listed in the figures and then i.v. injected into LPS-induced acute skin inflammatory mice (F) or CT26 tumor-bearing mice (G). DiR dye signals in skin and tumor tissues were determined 24 hours after the injection. H, transmigration of IGNVs with/without LFA-1 neutralization. PKH26-labeled IGNVs were preincubated overnight with anti-LFA-1 antibody at 4°C and then added into the apical chamber. The intensity of PKH26 fluorescence of the media in the lower chamber was measured after 24 and 48 hours of incubation and expressed as the percentage of Transwell efficiency of $PKH26^+$IGNVs. I, DiR dye-labeled IGNVs were preincubated with functional anti-LFA-1 antibody at 4°C overnight, washed, i.v. injected into LPS-induced acute skin inflammatory mice and the DiR signals was detected after 24-hour injection. A representative image (F, G, and I) from each group of mice ($n = 5$) 24 hours after the injection is shown and graphical figures are presented as the mean net intensity (sum intensity/area, $n = 5$). *, $P < 0.05$; **, $P < 0.01$; and ***, $P < 0.001$. Data are the mean ± SEM. of at least three independent experiments.

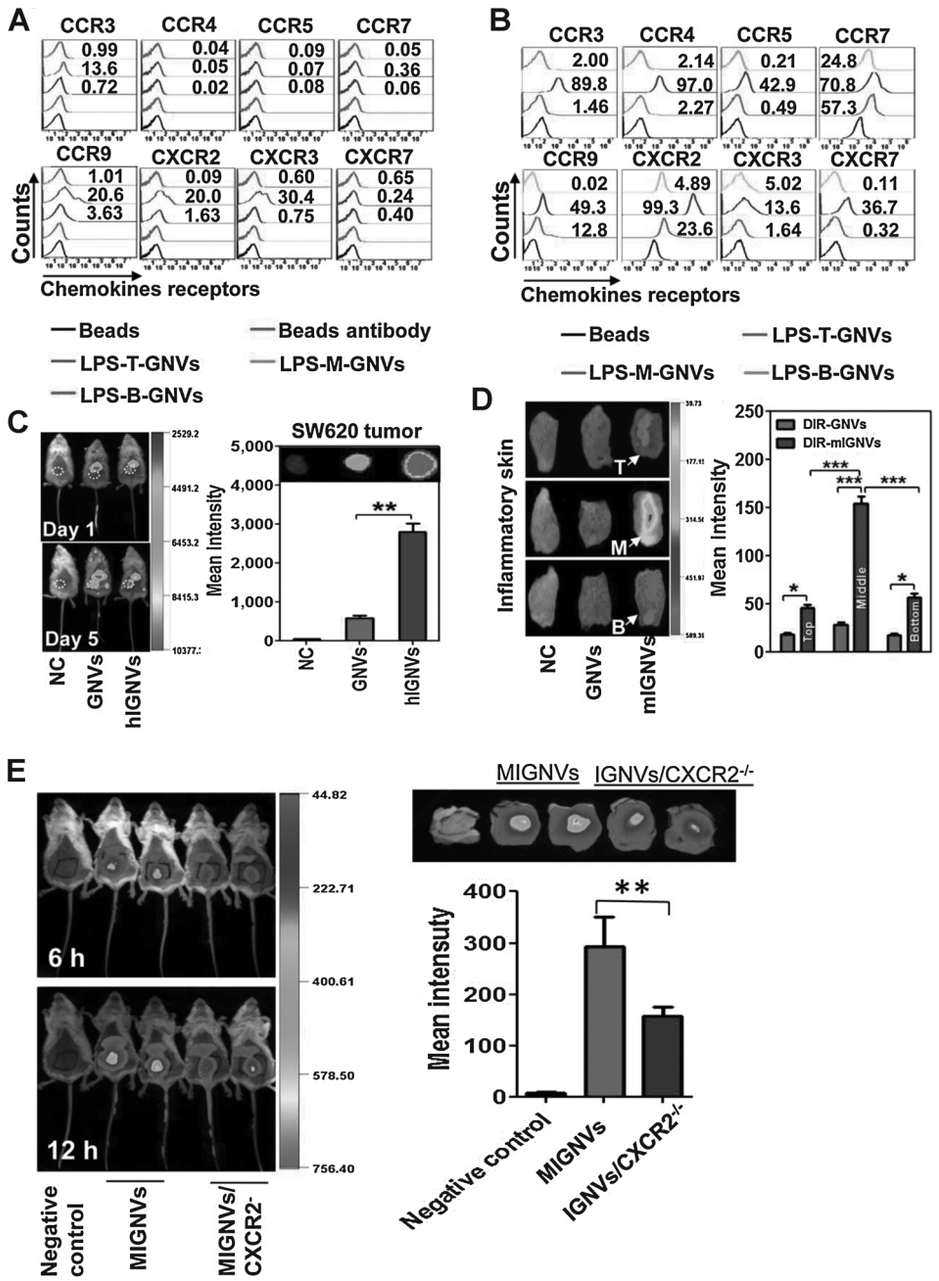

Figure 4.
Targeting to human colon cancer by coating GNVs with the plasma membrane of LPS-stimulated leukocytes isolated from peripheral blood of healthy human subjects (hIGNVs) or of mice (mIGNVs). Profiles of hIGNV (A) and mIGNV (B) chemokine receptors are shown based on FACS analysis. Representative histograms ($n = 5$) show the percentage of staining of chemokine receptors from the hIGNVs and mIGNVs. Three different bands from sucrose gradients of plasma membrane from LPS-stimulated leukocytes were used for coating GNVs. Top band (LPS-T), middle band (LPS-M), and bottom band (LPS-B). C, trafficking of DiR dye-labeled hIGNVs in human colon cancer SW620-bearing mice. Mice were i.v. injected with DiR dye-labeled hIGNVs. Live imaging of whole mice was carried out on days 1 and 5 after the injection. At day 5, after the injection, tumors were removed and scanned. Trafficking of DiR dye-labeled–mIGNVs in LPS-induced acute skin inflammatory mouse model were measured. Mice were i.v. injected with DiR dye-labeled mIGNVs without (D) or with (E) CXCR2 knockout. Skin was removed 72 hours (D) or 24 hours (E) after the injection and scanned. A representative image (C and D) from each group of mice is shown and graphical figures are presented as the mean net intensity (sum intensity/area, $n = 5$). *, $P < 0.05$; **, $P < 0.01$; and ***, $P < 0.001$. Data are the mean ± SEM. of at least three independent experiments (C, D, and E).

IGNVs, is required for higher efficiency delivery of DOX to inflammatory sites. The biologic effects of IGNV-DOX on the CT26 colon tumor and 4T1 breast tumor models were also significant when compared with the other treatments. IGNV-DOX treatment led to significant inhibition in the growth of CT26 and 4T1 tumor (Fig. 5E; *, $P < 0.05$; **, $P < 0.01$; and ***, $P < 0.001$) and extended the survival of tumor-bearing mice (Fig. 5F; *, $P < 0.05$ and **, $P < 0.01$). The results from IGNV-Cur treatment of DSS-induced mouse colitis also indicated that IGNVs carrying curcumin has a better therapeutic effect on the inhibition of colitis than GNVs carrying curcumin or curcumin alone. This conclusion is supported by the fact that there was less blood in stools (Supplementary Fig. S8B), there was less weight loss (Supplementary Fig. S8C), there was a significantly improved survival rate (Supplementary Fig. S8D) in DSS-induced colitis mice i.v. injected with IGNV-Cur than control groups as listed, and fewer leukocytes were observed infiltrating hematoxylin and eosin-stained mouse colon tissue (Supplementary Fig. S8E). These results were also consistent with higher concentrations of curcumin detected in the colon tissues of mice treated with IGNV-Cur (Supplementary Fig. S8F). ELISA analysis further indicated that significantly less TNFα, IL6 and IL1β were detected in the colon tissue extracts of DSS-induced colitis mice i.v. injected with IGNV-Cur than with PBS/DSS, free Cur, or GNV-Cur (Supplementary Fig. S8G).

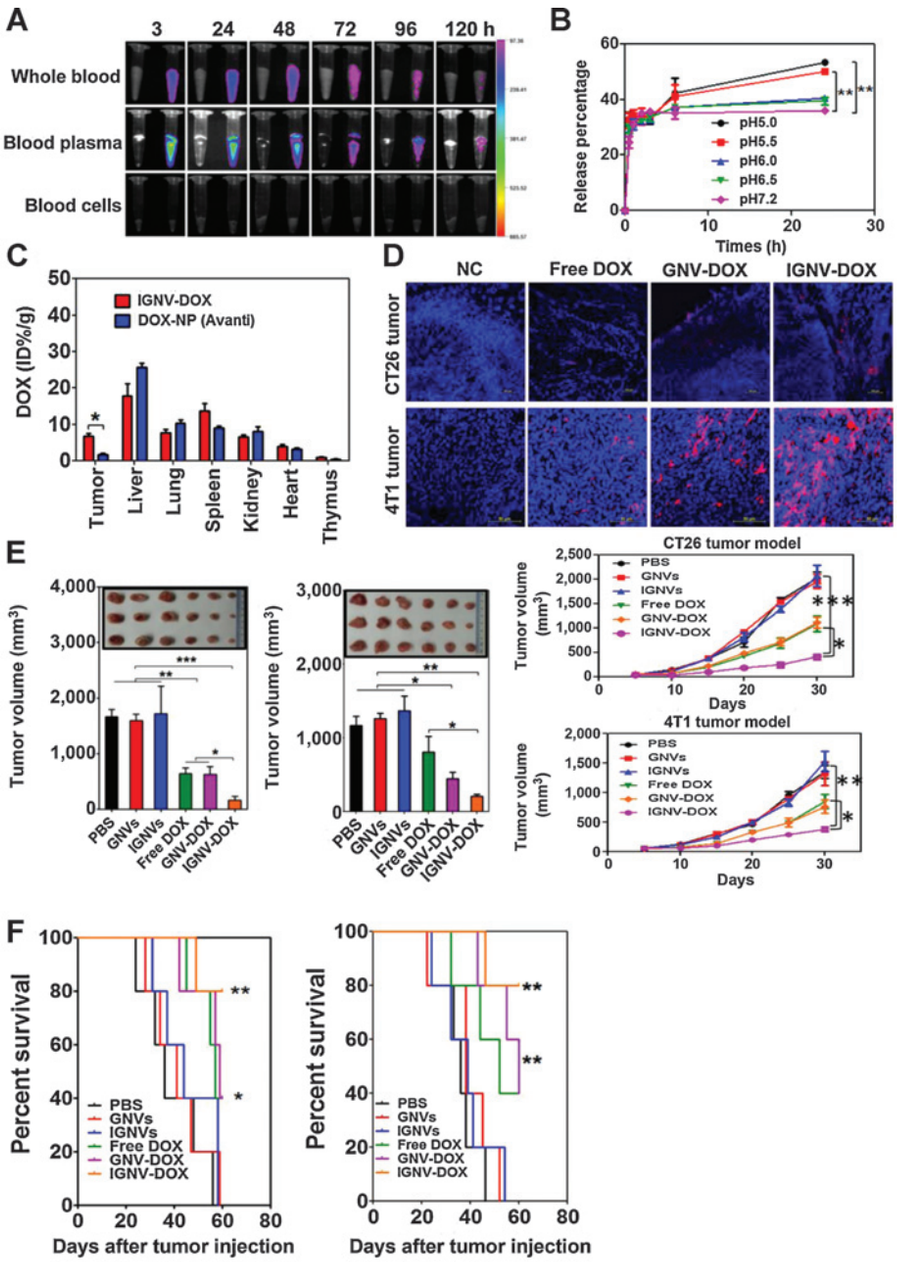

Figure 5.
Targeted therapeutic drug delivery for mouse cancer. A, stability of circulating IGNVs. Representative images ($n = 3$) are shown. B, *in vitro* release profile of doxorubicin from IGNV-DOX in PBS buffer with different pH values (5.0, 5.5, 6.0, 6.5, and 7.2; $n = 5$). **, $P < 0.01$. C, biodistribution of doxorubicin in 4T1 tumor-bearing mice. 4T1 tumor-bearing mice ($n = 5$) were i.v. injected with IGNV-DOX or DOX-NP, and the doxorubicin in 4T1 tumor tissues, livers, lungs, spleens, kidneys, hearts, and thymus were measured. *, $P < 0.05$. Data (B and C) are the mean ± SEM of at least three independent experiments. D, biodistribution of doxorubicin in CT26 and 4T1 tumor tissues. Free doxorubicin (Free DOX), GNV-delivered doxorubicin (GNV-DOX) and IGNV-delivered doxorubicin (IGNV-DOX) were i.v. injected into CT26 ($n = 5$) and 4T1 tumor-bearing mice ($n = 5$). Tumor tissues were removed, fixed, and sectioned. Doxorubicin in tumor tissues was observed using a confocal imaging system. The images for one representative experiment of three are shown. E, CT26 and 4T1 cells were injected subcutaneously (CT26) or in a mammary fat pad (4T1) of BALB/c mice. Mice were i.v. injected with IGNV-DOX or controls as listed in the figure every 3 days for 30 days from 7 days after tumor cells were injected. Representative images of tumors (E, left) from each group ($n = 5$) are shown; tumor volume was measured every 5 days (E, right), and the survival rate (F) of mice was calculated. *, $P < 0.05$ and **, $P < 0.01$. Data are the mean ± SEM of at least three independent experiments (E and F).

Discussion

Our study advances an approach for targeted delivery of therapeutic agents to inflammatory sites where the appropriate cells are targeted; thereby promoting much more substantial therapeutic benefits without inducing adverse side effects. We show that IGNVs can be an effective, personalized approach to potentially treat patients with a variety of inflammatory conditions. The use of IGNVs avoids several of the problems that have arisen with conventional therapy vectors, such as the lack of tissue targeting specificity, immunogenicity, difficulty in scalability and production, and the need for life-long monitoring for tumorigenesis and other adverse clinical outcomes. Because IGNVs do not cause these concerns, they have great potential as targeted delivery vehicles, in particular, because production of GNVs is easily scaled up and the GNVs can be coated with leukocyte membranes from an individual making this approach personalized and economically feasible for treatment of patients in low and middle income countries where they do not have comprehensive facilities to make synthetic therapeutic vectors.

To successfully target a specific tissue, four goals must be met: (i) extended circulation of the delivery vector, (ii) tissue penetration by the vector, (iii) tissue specificity, and (iv) release of the payload, that is, the therapeutic agent. Tumor tissues have abnormal molecular and fluid transport dynamics, especially for

macromolecular drugs. This phenomenon is referred to as the "enhanced permeability and retention (EPR) effect" of macromolecules and lipids in solid tumors (19, 20). Therefore, the longer the vector is in the circulation, the greater opportunity it has to penetrate the tumor tissue by utilizing the EPR effect. Our previously published work shows that a nanovector made of lipids from grapefruit nanoparticles circulates in the peripheral blood more than 5 days in tumor-bearing mice (18). GNVs are stable in the circulatory system and thus have a greater opportunity to enter the tumor tissue. In addition, the critical concentration of grapefruit nanoparticle-derived lipids for GNV formation was 1.5 μmol/L (Supplementary Fig. S9), and GNVs do not increase in size with increasing concentrations of total lipids up to 5 μmol/L. The diameter of GNVs at 25 μmol/L to 50 μmol/L concentration and at 25°C is increased up to 200 nm, and retained at 200 nm, whereas lipid concentration was further increased up to 100 μmol/L. We believe that this finding not only provides a guideline for selecting concentrations of grapefruit nanoparticle-derived lipids to make desirable sized GNVs (50–200 nm), but also a broad range of concentrations of grapefruit nanoparticle-derived lipids can be selected for making GNVs without leading to a further increase of GNV size. The latter feature has an advantage in case that a large amount of grapefruit nanoparticle-derived lipids is required to make GNVs, which allows for higher concentrations of therapeutic agents to be encapsulated per GNV. However, this feature of GNVs alone may not be sufficient to deliver ample agent to the targeted tissue to have a therapeutic effect. Achieving specific and safe delivery of a drug across endothelial cells is essential before it is to reach the targeted tissue. However, due to the fact that most delivery vectors lack an affinity for endothelium, only a small fraction of therapeutics can be delivered to the targeted tissue by utilizing the EPR effect. In this study, we modified IGNVs so that they could take advantage of the activated leukocyte pathway that is primarily driven by leukocyte recruitment-related factors, including chemokines/chemokine receptors, and integrins by coating the IGNVs with the membranes from activated leukocytes. This modification of IGNVs significantly enhanced their endothelial cell transmigration capability so the IGNVs could enter inflammatory tissues. As we demonstrated in this study, not only can this strategy be applied to breast cancer and colon cancer, but also the potential exist that the IGNVs could be used to treat many different types of diseases since the inflammatory process is a hallmark of many chronic diseases, including cancer, infectious diseases, and autoimmune diseases. As shown in this study, the chemotherapy drug doxorubicin and the anti-inflammatory agent curcumin can be delivered successfully by IGNVs to reach the desired inflammatory site and achieve a therapeutic effect through modification of GNVs with membranes of activated leukocytes from individuals. Specifically, we demonstrated that i.v. injection of IGNV-DOX or IGNV-Cur significantly enhances the inhibition of breast tumor and colon tumor growth, and attenuates DSS-induced colitis, respectively. This response was due to improved recruitment of IGNVs into tumor as well as inflamed colon tissue. The membranes from activated leukocytes were required to obtain this benefit, as it permitted IGNV delivery to the precise place where inflammation was occurring.

We expect that other factors in addition to chemokines/chemokine receptors may also play a role in IGNVs homing to an inflammatory site. The results published by another group suggest that LFA-1 plays a role in the nanoparticle homing to an inflamed site (10). We used LFA-1 (CD11a–CD18) as an example. Our data also showed that CXCR2 and LFA-1 played a role in the transmigration of IGNVs as demonstrated in an *in vitro* Transwell blocking assay and *in vivo* skin inflammatory mouse model. Therefore, the role of IGNV chemokine receptors as demonstrated in this study does not exclude a number of other IGNV factors, such as CXCR2 and LFA-1, which also plays a role in the process of IGNV recruitment into inflamed tissue. This is also the reason that we believe that IGNVs coated with total leukocyte membranes may have a greater potential for being applied to personalized medicine for targeted delivery to inflammatory sites than the use of individual chemokine receptor coated IGNVs. It is conceivable that membrane-associated chemokine and integrin profiles of circulating inflammatory cells from patients with different chronic inflammatory diseases may be different in their makeup. Furthermore, individual chemokine receptor-coated GNVs may be potentially difficult to optimize in combinations or as a customized set or group of chemokine receptors that are most suitable for targeted delivery for an individual patient. In addition, there may be a higher cost for production of recombinant chemokine receptors and recombinant production would require FDA approval for clinical use. Finally, potential biosafety issues could arise due to using synthesized recombinant chemokine receptors.

An ideal delivery vehicle should be susceptible to manipulation so delivered therapeutic drugs can be released within the targeted tissue. Evidence accumulated over the past decades has shown that the pH in electrode-evaluated human tumor is on average lower than the pH of normal tissues (21–24). Our results presented in this study show that doxorubicin encapsulated in the IGNVs is stable until the pH drops to 6.0 or below. This feature of IGNVs allows the encapsulated drug to selectively be released in tumor tissue, and therefore reduces the side effects seen when chemotherapy treatment nondiscriminately affects healthy organs and tissues, which is one of major obstacles for chemotherapy for treatment of patients with cancer.

In the past decades, substantial experimental and clinical evidence supports the conclusion that one of the most important mechanisms operating in tumor progression involves chemokines and their receptors (25, 26). Chemokines and their receptors not only play a role in cancer-related inflammation, but also have been implicated in the invasiveness and metastasis of diverse cancers (25, 27, 28). We speculate that pseudo-inflammatory chemokine receptors delivered by GNVs may also act as soluble receptors to block the pathway(s) mediated by chemokine receptors expressed on the tumor cells or other tumor-associated cells. This assumption is currently under examination in our laboratories, and if this is a case, not only could this delivery strategy be applied to targeted delivery as demonstrated in this study, but also could prove useful in treating a number of chemokine/chemokine receptor-associated diseases.

Disclosure of Potential Conflicts of Interest

No potential conflicts of interest were disclosed.

Authors' Contributions

Conception and design: Q. Wang, D. Miller, H.-G. Zhang
Development of methodology: Q. Wang, Y. Ren, J. Mu, X. Zhuang, L. Zhang, J. Yan, D. Miller, H.-G. Zhang
Acquisition of data (provided animals, acquired and managed patients, provided facilities, etc.): Q. Wang, Y. Ren, H.-G. Zhang

Analysis and interpretation of data (e.g., statistical analysis, biostatistics, computational analysis): Q. Wang, Y. Ren, H.-G. Zhang
Writing, review, and/or revision of the manuscript: Q. Wang, N.K. Egilmez, H.-G. Zhang
Administrative, technical, or material support (i.e., reporting or organizing data, constructing databases): Q. Wang, J. Mu, X. Zhuang, Z. Deng, L. Zhang, H.-G. Zhang
Study supervision: H.-G. Zhang

Acknowledgments

The authors thank Dr. Jerald Ainsworth for editorial assistance.

Grant Support

This work was supported by grants from NIH (UH2TR000875) and the Louisville Veterans Administration Medical Center (VAMC) Merit Review Grants (H.-G. Zhang).

The costs of publication of this article were defrayed in part by the payment of page charges. This article must therefore be hereby marked *advertisement* in accordance with 18 U.S.C. Section 1734 solely to indicate this fact.

Received October 24, 2014; revised February 24, 2015; accepted March 16, 2015; published OnlineFirst April 16, 2015.

References

1. Kugelberg E. T cell responses: kiss and run. Nat Rev Immunol 2014;14:134.
2. Pober JS, Sessa WC. Evolving functions of endothelial cells in inflammation. Nat Rev Immunol 2007;7:803–15.
3. Schall TJ, Proudfoot AE. Overcoming hurdles in developing successful drugs targeting chemokine receptors. Nat Rev Immunol 2011;11:355–63.
4. Mantovani A, Bonecchi R, Locati M. Tuning inflammation and immunity by chemokine sequestration: decoys and more. Nat Rev Immunol 2006;6:907–18.
5. Ben-Baruch A. Organ selectivity in metastasis: regulation by chemokines and their receptors. Clin Exp Metastasis 2008;25:345–56.
6. Godessart N. Chemokine receptors: attractive targets for drug discovery. Ann N Y Acad Sci 2005;1051:647–57.
7. Warnock RA, Campbell JJ, Dorf ME, Matsuzawa A, McEvoy LM, Butcher EC. The role of chemokines in the microenvironmental control of T versus B cell arrest in Peyer's patch high endothelial venules. J Exp Med 2000;191:77–88.
8. Weber M, Uguccioni M, Baggiolini M, Clark-Lewis I, Dahinden CA. Deletion of the NH2-terminal residue converts monocyte chemotactic protein 1 from an activator of basophil mediator release to an eosinophil chemoattractant. J Exp Med 1996;183:681–5.
9. O'Hayre M, Salanga CL, Handel TM, Hamel DJ. Emerging concepts and approaches for chemokine-receptor drug discovery. Expert opin Drug Discov 2010;5:1109–22.
10. Parodi A, Quattrocchi N, van de Ven AL, Chiappini C, Evangelopoulos M, Martinez JO, et al. Synthetic nanoparticles functionalized with biomimetic leukocyte membranes possess cell-like functions. Nat Nanotechnol 2013;8:61–8.
11. Hock SC, Ying YM, Wah CL. A review of the current scientific and regulatory status of nanomedicines and the challenges ahead. PDA J Pharm Sci Technol 2011;65:177–95.
12. Juliano R. Nanomedicine: is the wave cresting? Nat Rev Drug Discov 2013;12:171–2.
13. Zhuang X, Xiang X, Grizzle W, Sun D, Zhang S, Axtell RC, et al. Treatment of brain inflammatory diseases by delivering exosome encapsulated anti-inflammatory drugs from the nasal region to the brain. Mol Ther 2011;19:1769–79.
14. Alvarez-Erviti L, Seow Y, Yin H, Betts C, Lakhal S, Wood MJ. Delivery of siRNA to the mouse brain by systemic injection of targeted exosomes. Nat Biotechnol 2011;29:341–5.
15. Wang B, Zhuang X, Deng ZB, Jiang H, Mu J, Wang Q, et al. Targeted drug delivery to intestinal macrophages by bioactive nanovesicles released from grapefruit. Mol Ther 2014;22:522–34.
16. Ju S, Mu J, Dokland T, Zhuang X, Wang Q, Jiang H, et al. Grape exosome-like nanoparticles induce intestinal stem cells and protect mice from DSS-induced colitis. Mol Ther 2013;21:1345–57.
17. Mu J, Zhuang X, Wang Q, Jiang H, Deng ZB, Wang B, et al. Interspecies communication between plant and mouse gut host cells through edible plant derived exosome-like nanoparticles. Mol Nutr Food Res 2014;58:1561–73.
18. Wang Q, Zhuang X, Mu J, Deng ZB, Jiang H, Zhang L, et al. Delivery of therapeutic agents by nanoparticles made of grapefruit-derived lipids. Nat Commun 2013;4:1867.
19. Maeda H, Wu J, Sawa T, Matsumura Y, Hori K. Tumor vascular permeability and the EPR effect in macromolecular therapeutics: a review. J Control Release 2000;65:271–84.
20. Maeda H, Matsumura Y. Tumoritropic and lymphotropic principles of macromolecular drugs. Crit Rev Ther Drug Carrier Syst 1989;6:193–210.
21. Gerweck LE, Seetharaman K. Cellular pH gradient in tumor versus normal tissue: potential exploitation for the treatment of cancer. Cancer Res 1996;56:1194–8.
22. Chen H, Liu X, Dou Y, He B, Liu L, Wei Z, et al. A pH-responsive cyclodextrin-based hybrid nanosystem as a nonviral vector for gene delivery. Biomaterials 2013;34:4159–72.
23. Li P, Liu D, Miao L, Liu C, Sun X, Liu Y, et al. A pH-sensitive multifunctional gene carrier assembled via layer-by-layer technique for efficient gene delivery. Int J Nanomed 2012;7:925–39.
24. Mok H, Veiseh O, Fang C, Kievit FM, Wang FY, Park JO, et al. pH-Sensitive siRNA nanovector for targeted gene silencing and cytotoxic effect in cancer cells. Mol Pharm 2010;7:1930–9.
25. Reymond N, d'Agua BB, Ridley AJ. Crossing the endothelial barrier during metastasis. Nat Rev Cancer 2013;13:858–70.
26. Balkwill F. Cancer and the chemokine network. Nat Rev Cancer 2004;4:540–50.
27. Lombardi L, Tavano F, Morelli F, Latiano TP, Di Sebastiano P, Maiello E. Chemokine receptor CXCR4: role in gastrointestinal cancer. Crit Rev Oncol Hematol 2013;88:696–705.
28. Franciszkiewicz K, Boissonnas A, Boutet M, Combadiere C, Mami-Chouaib F. Role of chemokines and chemokine receptors in shaping the effector phase of the antitumor immune response. Cancer Res 2012;72:6325–32.